Effect of starting particle size on hot-pressing of magnesium oxide powder prepared by vapour-phase oxidation process

K. ITATANI, R. YASUDA, F. SCOTT HOWELL, A. KISHIOKA
Department of Chemistry, Faculty of Science and Engineering, Sophia University, 7-1 Kioi-cho, Chiyoda-ku, Tokyo 102 Japan

Effect of starting particle size on hot-pressing of magnesium oxide (MgO) powder was examined using seven kinds of MgO powders prepared by a vapour-phase oxidation process; the average primary particle sizes were 11, 25, 32, 44, 57, 107 and 261 nm. These compressed powders (compacts) were hot-pressed at a temperature between 900 and 1300 °C. The densifications of these compacts during the hot-pressing proceeded via (i) the sintering of primary particles within secondary particles and the rearrangement of secondary particles/grains (900 °C), (ii) the gradual grain growth controlled by the pore migration (900 ~1100 °C) and (iii) the rapid grain growth due to the active mass transfer (1300 °C); the grain sizes of MgO compacts hot-pressed at and below 1100 °C were $< 1\,\mu m$, while those at 1300 °C attained 20 ~30 μm. The transluscent compact with the relative density of 99.7% could be obtained when the compressed powder with the average primary particle size of 44 nm was hot-pressed at a temperature as low as 1100 °C for 1 h.

1. Introduction

The properties of magnesium oxide (MgO) powder prepared by a vapour-phase oxidation process are characterized as follows: (i) high purity (over 99.9 %), (ii) submicrometre-sized particles, (iii) narrow particle size distribution and (iv) "soft" agglomerates [1]. By making use of these MgO powders, some of us reported that dense MgO ceramics with the relative densities of ~98 % can be fabricated by the pressureless sintering [2, 3] and that the bending strength of such MgO ceramics can attain a value of ~183 MPa [4].

As a next step, we examined the hot-pressing conditions for fabricating the dense MgO ceramics. The hot-pressing technique is effective for fabricating dense MgO ceramics at lower temperatures than the pressureless sintering technique. Although the hot-pressing of MgO powders prepared by the vapour-phase oxidation process has once been carried out by Yasuda *et al.* [5], the effect of starting particle size on hot-pressing of such MgO powders has never been available yet. In this paper, we describe the fabrication of the dense MgO ceramics by the hot-pressing technique, using seven kinds of MgO powders with the average primary particle sizes of 11 to 261 nm prepared by the vapour-phase oxidation process.

2. Experimental procedure

Seven kinds of MgO powders prepared by the vapour-phase oxidation process were provided by Ube Industries, Ltd. The average primary particle sizes of the powders calculated on the basis of the specific surface areas were 11, 25, 32, 44, 57, 107 and 261 nm; these powders were designated as A(11), B(25), C(32), D(44), E(57), F(107) and G(261), respectively [3, 4].

The particle shapes of the starting powders were observed using a transmission electron microscope (TEM: Model H-300, Hitachi, Tokyo). The samples for TEM observation were made by putting the powders on the carbon film supported by copper grid. The agglomerate-size distributions of the starting powders were measured using a laser diffraction particle size analyser (Model SALD-1100, Shimadzu, Kyoto, Japan). Ethanol was used as a dispersion medium.

The cylindrical compacts with diameters of 5 mm and thickness of ~3 mm were fabricated by pressing ~0.15 g of the powders uniaxially at 294 MPa. The expansion–shrinkages of the compacts were measured from room temperature up to 1400 °C at the heating rate of 10 °C min^{-1}; the shrinkage rates of the compacts were calculated using a personal computer.

The cylindrical compacts with diameters of 20 mm and thickness of ~2 mm were fabricated by pressing ~1.5 g of the powder uniaxially at 30 MPa. The compacts were set in a silicon nitride (Si_3N_4) die and were hot-pressed at a temperature between 900 and 1300 °C under the pressure of 30 MPa; the atmosphere was selected to be nitrogen (N_2) to prevent the die from oxidation. The heating rate was 5 °C min^{-1}. After hot-pressing for the desired time, the compacts were cooled down to 300 °C at the rate of 5 °C min^{-1} and then the electric power was turned off.

0022–2461

The polished surfaces of the hot-pressed compacts, which had been etched thermally at 50 °C lower than the firing temperature, were observed using a scanning electron microscope (SEM: Model S-430, Hitachi, Tokyo). On the basis of the SEM micrographs, the grain sizes were calculated by an intercept method [6].

3. Results and discussion

3.1. Properties of the starting MgO powders

The typical particle shapes and agglomerate-size distributions are shown in this section. Since we have previously reported some of the powder properties, such as specific surface area, crystallite size, primary particle size and secondary particle size [2, 3], we continue the discussion by comparing the present and previous data.

Fig. 1 shows typical TEM micrographs of Powders B(25) and E(57). Powder B(25) contained the cubic-shaped particles and the corner-rounded particles with sizes below 0.1 μm (100 nm) (Fig. 1a). The particle shapes of Powder E(57) were similar to those of Powder B(25); however, the particle sizes were below 0.15 μm (150 nm) (Fig. 1b).

Our previous research revealed that the above cubic-shaped and corner-rounded particles correspond to the primary particles and that these particles are single crystals [2, 3]. The cubic shape of each particle reflects the cubic crystal system of MgO.

Next the agglomerate sizes of these powders were measured using the laser diffraction particle size analyser. Note that the measured agglomerate sizes do not precisely correspond to the agglomerate sizes of the powders handled in air, because the measurement was performed by dispersing the powders in ethanol [7]. Nevertheless, this technique is useful for evaluating the agglomeration states of the powders when the agglomerate sizes of the powders are measured under the same conditions. The measured data are shown in Fig. 2. The distribution curves of these powders are classified into two, according to the primary particle size: (a) Powders A(11)–C(32) and (b) Powders D(44)–G(261).

The agglomerate sizes of Powders A(11)–C(32) were in the ranges of 0.1 to 0.5 μm and 0.5 to 10 μm (Fig. 2a). Although the above average primary particle sizes are in the range of 11 to 32 nm (0.011–0.032 μm), the agglomerate sizes distribute over the range of 0.1 to 10 μm. Thus most of the primary particles are adhered to form agglomerates. The agglomerates with sizes ranging from 0.1 to 0.5 μm correspond to the secondary particles, because our previous SEM observation indicated that the spherical agglomerates (secondary particles) with sizes of $\leqslant 0.5$ μm are present in these powders [3]. The secondary particles are furthermore adhered to form ternary particles with sizes of 1 to 5 μm. The frequencies of these ternary particles increase with decreasing the primary particle size. This phenomenon is interpreted as follows: although the primary particles may spontaneously adhere to one another to form secondary particles, the huge surface energies which ultrafine powders possess cannot be easily lowered down until the secondary particles adhere to one another to form ternary particles. The presence of the "hard" agglomerates or strongly-coagulated primary particles in Powder A(11) has been confirmed by Nishida *et al.* [8], who reported that these agglomerates start to fracture at ~ 30 MPa.

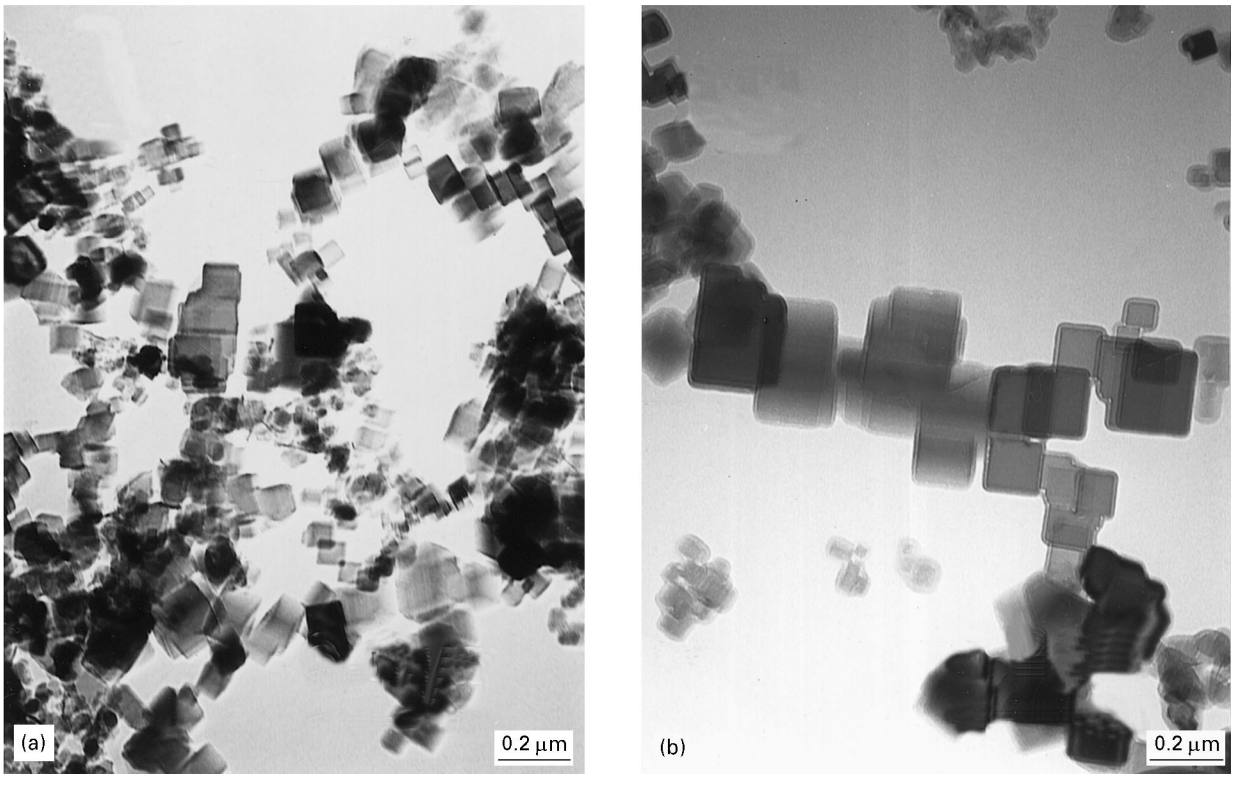

Figure 1 Typical TEM micrographs of (a) Powder B(25) and (b) Powder E(57).

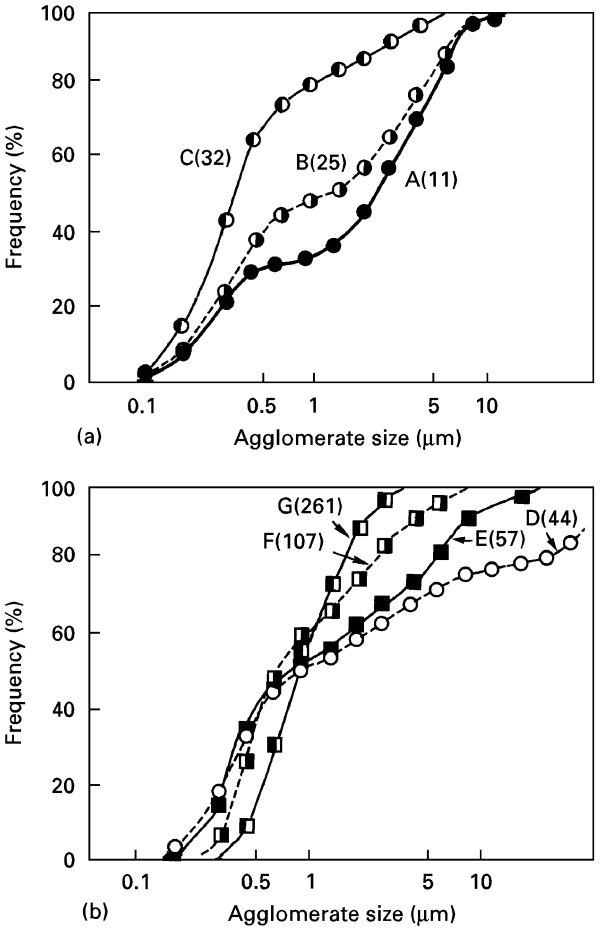

Figure 2 Agglomerate-size distributions of Powders A(11) to G(261).

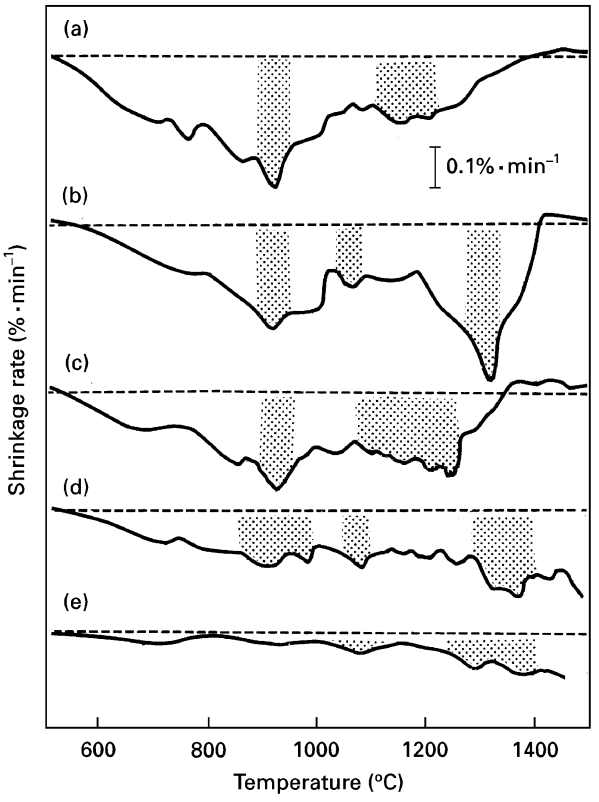

Figure 3 Changes in shrinkage rates of (a) Compact A(11), (b) Compact B(25), (c) Compact D(44), (d) Compact E(57) and (e) Compact G(261) at the heating rate of 10 °C min^{-1}. The shaded regions indicate the parts where the shrinkage rates are accelerated.

The agglomerate sizes of Powders D(44) and E(57) were in the ranges of 0.1 to over 10 μm, whereas those of Powders F(107) and G(261) were in the range of 0.1 to 10 μm (Fig. 2b). The secondary particles in Powders D(44) and E(57) can no longer be clearly distinguished from ternary particles, due to the weak coagulation forces among the primary particles. The agglomerate-size distributions of Powders F(107) and G(261) are narrower than those of Powders D(44) and E(57), which suggests that Powders F(107) and G(261) do not contain ternary particles, but only secondary particles.

3.2. Densification process of MgO compact during heating

We evaluated the densification processes of the present powders during heating. Since we measured the shrinkage curves of Compacts A(11)–G(261) during the heating, the shrinkage rates of these compacts were calculated on the basis of those shrinkage data. Typical results are shown in Fig. 3. The overall trend revealed that the shrinkage rates of Compacts A(11) to G(261) reached maximum values at ~900 °C, ~1100 °C and ~1300 °C, although the maximum values varied slightly according to the changes in primary particle size.

The maximum value at ~900 °C indicates the sintering of primary particles at the initial stage [3]. On the basis of the above results, the initial sintering behaviour of these powders were examined by measuring the isothermal shrinkages of the compacts in the temperature range of 600 to 1000 °C. The relationship between isothermal shrinkage ($\Delta L/L_0$) ($\Delta L(= L_0 - L_t)$, L_0: initial thickness, L_t: thickness at time = t) and sintering time (t) is expressed as follows [9]

$$\frac{\Delta L}{L_0} = \left(\frac{K'\gamma a^3 D}{kTr^p}\right)^m t^m \quad (1)$$

where γ represents surface energy, a^3 vacancy volume, D diffusion coefficient for the rate controlling species, k Boltzmann's constant, T absolute temperature, r particle radius, and K', m, p are constants depending upon the diffusion path. Assuming that the parameters in the parentheses can be regarded as constants (= C), the logarithmic relationship between shrinkage ($\Delta L/L_0$) and time (t) is expressed as follows

$$\log\left(\frac{\Delta L}{L_0}\right) = m\log t + m\log C \quad (2)$$

The diffusion path may be anticipated from the slope (m) of this straight line. Then we incorporated our data into Equation 2 to search for the best fitted m value. A typical logarithmic relationship between isothermal shrinkage and time of the compact is shown in Fig. 4. The shrinkages of Compacts A(11) and D(44) increased exponentially with time. The former slope was

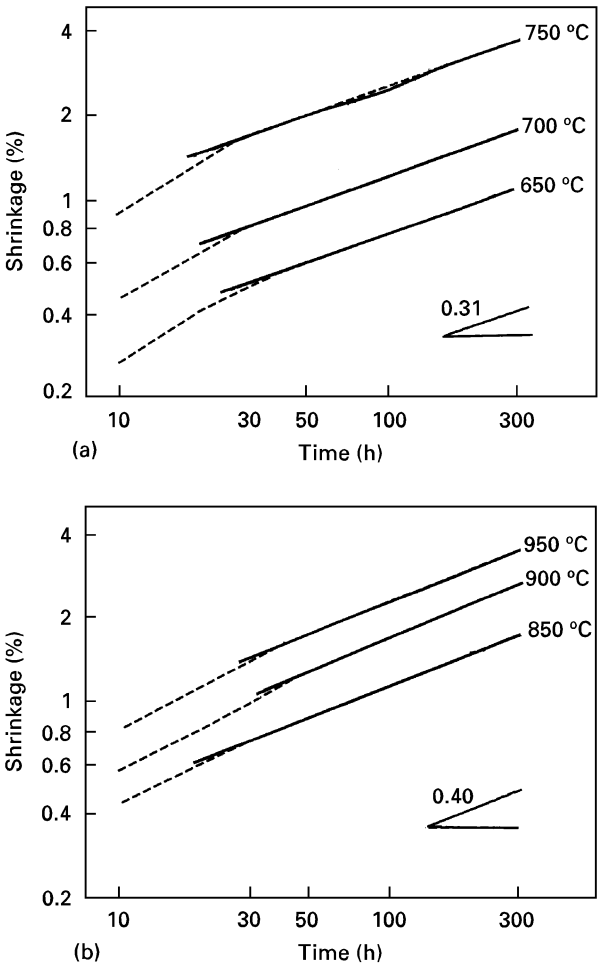

Figure 4 Typical isothermal shrinkage curves of (a) Compact A(11) and (b) Compact D(44).

estimated to be 0.31, the latter slope to be 0.40. Although other data were omitted in this paper, the overall trend revealed that the slope of 0.31 was obtained for the cases of Compacts A(11) and B(25), whereas the slope of 0.40 was usual for the cases of Compacts C(32)–G(261).

Wermuth and Knapp [10] report that the m value for the sintering of MgO powder with the primary particle size of $\sim$20 nm ranges from 0.33 to 0.35, in agreement with the boundary diffusion model [9]. On the other hand, Hamano *et al.* [11] and Yamaguchi *et al.* [12] report m values to be 0.40 and 0.50, respectively, in agreement with the bulk diffusion model [9, 13]. Comparing the present m values with those reported by the previous researchers, the mass transfer of Compacts A(11) and B(25) may be controlled by the boundary diffusion, the mass transfer of Compacts C(32)–G(261) by the bulk diffusion [9, 13]. The diffusion route changes with decreasing primary particle size from 32 down to 25 nm. The boundary diffusion in the cases of Compacts A(11) and B(25) suggests that the mass transfer through the particle boundaries may be promoted with decreasing the primary particle size down to 25 nm, due to the presence of innumerable defects on and near the surfaces of these ultrafine primary particles. The presence of such defects may be confirmed by the fact that the lattice parameter of Powder A(11) increases from 0.4211 nm up to 0.4216 nm with decreasing the primary particle size down to 11 nm [8], because the weakening of Mg–O bond due to the presence of the defects must widen the interatomic distances.

On the basis of the isothermal shrinkage data, the apparent activation energies for the initial sintering are found from calculations to be $\sim$167 kJ mol^{-1} in the cases of Compacts A(11) and B(25), whereas they are $\sim$251 kJ mol^{-1} in the cases of Compacts C(32)–G(261). Wermuth and Knapp report the activation energy to be 252.8 kJ mol^{-1} for the MgO powder with the primary particle size as small as $\sim$20 nm [10]. This value is much higher than the present values ($\sim$167 kJ mol^{-1}) but is almost the same as the values ($\sim$251 kJ mol^{-1}) in the cases of Compacts C(32)–G(261). Such discrepancy may be explained by assuming that the present powder has a larger number of defects, due to which the activation energy is lowered.

Although Rhodes pointed out the interference of the strongly-bonded "aggregates" with initial stage of sintering [14], we consider that the effect of the agglomeration on initial stage of sintering may be neglected in this paper by the following reasons: (i) the initial stage of sintering is essentially affected by the surface areas or primary particle sizes; (ii) the present primary particles are not chemically bonded but only physically coagulated, as is evidenced by the presence of the cubic-shaped particles (see Fig. 1).

The maximum values at $\sim$1100 °C and $\sim$1300 °C, which appeared in the shrinkage rate curves of Compacts A(11)–E(57), may be associated with the sintering of grains. Details will be explained later.

3.3. Hot-pressing of MgO compact

The shrinkage data show that the maximum values of Compacts A(11)–E(57) appear at $\sim$900 °C, $\sim$1100 °C and $\sim$1300 °C. This fact suggests that the densifications of MgO compacts are accelerated at these temperatures. On the basis of this information, the compacts were hot-pressed at 900 °C, 1100 °C and 1300 °C. First the compacts were hot-pressed at 900 °C for 1 h; however, the hot-pressed compacts were fractured into several pieces when they were extruded from the dies. Since the hot-pressing time (1 h) at 900 °C was not sufficient for the fabrication of dense compacts, we changed the hot-pressing time from 1 h to 3 h; the hot-pressing time at 1100 °C and 1300 °C was fixed to be 1 h, because the dense MgO compacts could be obtained without prolonging the hot-pressing time until 3 h. The relative densities of the compacts fired at these temperatures are shown in Fig. 5 as a function of the primary particle size. When these compacts were hot-pressed at 900, 1100 and 1300 °C, the relative densities of the sintered compacts became maximal at the primary particle size of 44 nm; the highest relative density attained 99.7 % at 1100 °C. The relative density decreased as the primary particle size increased up to 261 nm.

Fig. 6 shows the appearance of Compact D(44) hot-pressed at 1100 °C for 1 h. The hot-pressed compact was translucent.

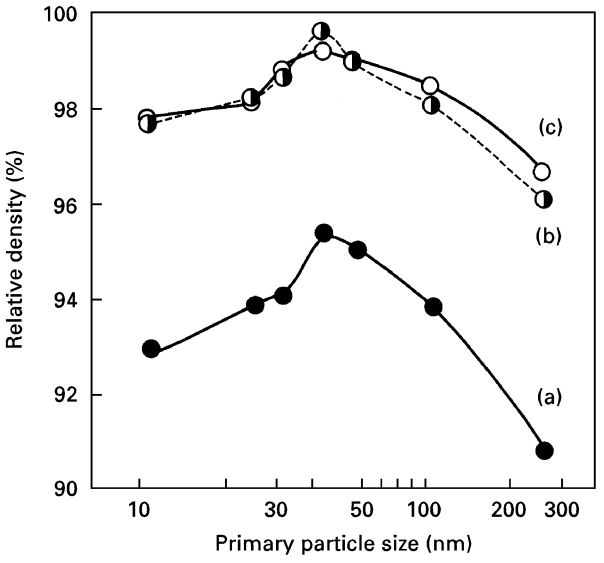

Figure 5 Relationship between primary particle size and relative density of the compact hot-pressed at (a) 900 °C for 3 h, (b) 1100 °C for 1 h and (c) 1300 °C for 1 h.

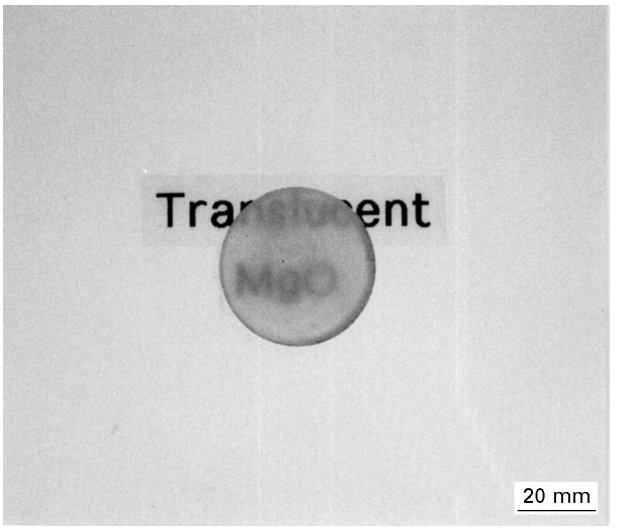

Figure 6 Appearance of Compact D(44) hot-pressed at 1100 °C for 1 h.

As described above, the relative density of Compact D(44) hot-pressed at 1100 °C for 1 h attains 99.7 %; the translucency of this compact proves that most of the pores are eliminated by hot-pressing Compact D(44) at this temperature. The present hot-pressing conditions and relative density of Compact D(44) are compared with those fabricated by the previous researchers [5, 15–21]. Although the relative densities vary according to the hot-pressing conditions (temperature, time and pressure) and starting particle properties, these researchers fabricated the translucent MgO compacts with relative densities of over 99 % at and above 1150 °C. Thus the present hot-pressing temperature of 1100 °C for fabricating the translucent Compact D(44) is lower than the temperatures employed by the previous researchers. The reason why Powder D(44) has such excellent sinterability may be that this powder contains submicrometre-sized primary particles (average size: 44 nm) and "soft" agglomerates [3].

The microstructures of these hot-pressed compacts were examined using SEM. SEM micrographs and grain-size distribution of Compact D(44) hot-pressed at 900 °C for 3 h are shown in Fig. 7, together with those of Compact D(44) hot-pressed at 900 °C for 1 h. Note that Compact D(44) hot-pressed at 900 °C for 1 h was broken into several pieces when it was extruded from the silicon-nitride die. The SEM micrograph of Compact D(44) hot-pressed at 900 °C for 1 h showed that the grains with sizes of ~0.2 μm were present and that the pores remained at the interfaces of grains (Fig. 7a); the histogram of the grain-size distribution showed that most of the grain sizes distributed over the range of 0.1 to 0.3 μm (Fig. 7a′). The SEM micrograph of Compact D(44) hot-pressed at 900 °C for 3 h showed that the grains with sizes of ~0.2 μm were packed closely (Fig. 7b); the histogram of the grain-size distribution showed that most of the grain sizes distributed below 0.4 μm (Fig. 7b′).

The average grain sizes of Compact D(44) hot-pressed at 900 °C for 1 h and 3 h are 0.17 μm and 0.19 μm, respectively. Little changes in average grain size are observed but the grains are more closely packed with time from 1 to 3 h. Since the above grain sizes are in accord with the average secondary particle size in Powder D(44), the densification may proceed via (i) the sintering of primary particles within secondary particles to form grains and (ii) the rearrangement of secondary particles/grains toward closer packing.

Fig. 8 shows the SEM micrographs and grain-size distributions of Compact D(44) hot-pressed at 1100 °C and 1300 °C for 1 h. The SEM micrograph of Compact D(44) hot-pressed at 1100 °C for 1 h showed that the polyhedral grains with sizes of ~0.5 μm were packed closely (Fig. 8a). The histogram of the grain-size distribution showed that the grain sizes distributed below 2.0 μm (Fig. 8a′). The SEM micrograph of Compact D(44) hot-pressed at 1300 °C for 1 h revealed that the polyhedral grains with sizes of ~20 μm were packed closely (Fig. 8b); the grain sizes distributed chiefly over the range of 10 ~40 μm (Fig. 8b′).

The average grain sizes of Compact D(44) hot-pressed at 1100 °C and 1300 °C for 1 h are 0.72 μm and 22.6 μm, respectively. Thus an increase in hot-pressing temperature brings about the appreciable grain growth.

Kuczynski [22] reported that the relationship between grain size (d) and porosity (p) may be expressed as follows

$$dp^n = K \quad (3)$$

where n and K represent constants. Equation 3 can also be expressed as follows

$$\log d = -n \log p + \log K \quad (4)$$

The present data are incorporated into Equation 4. Results are shown in Fig. 9. The data at 900 and 1100 °C were expressed as a straight line, whereas the

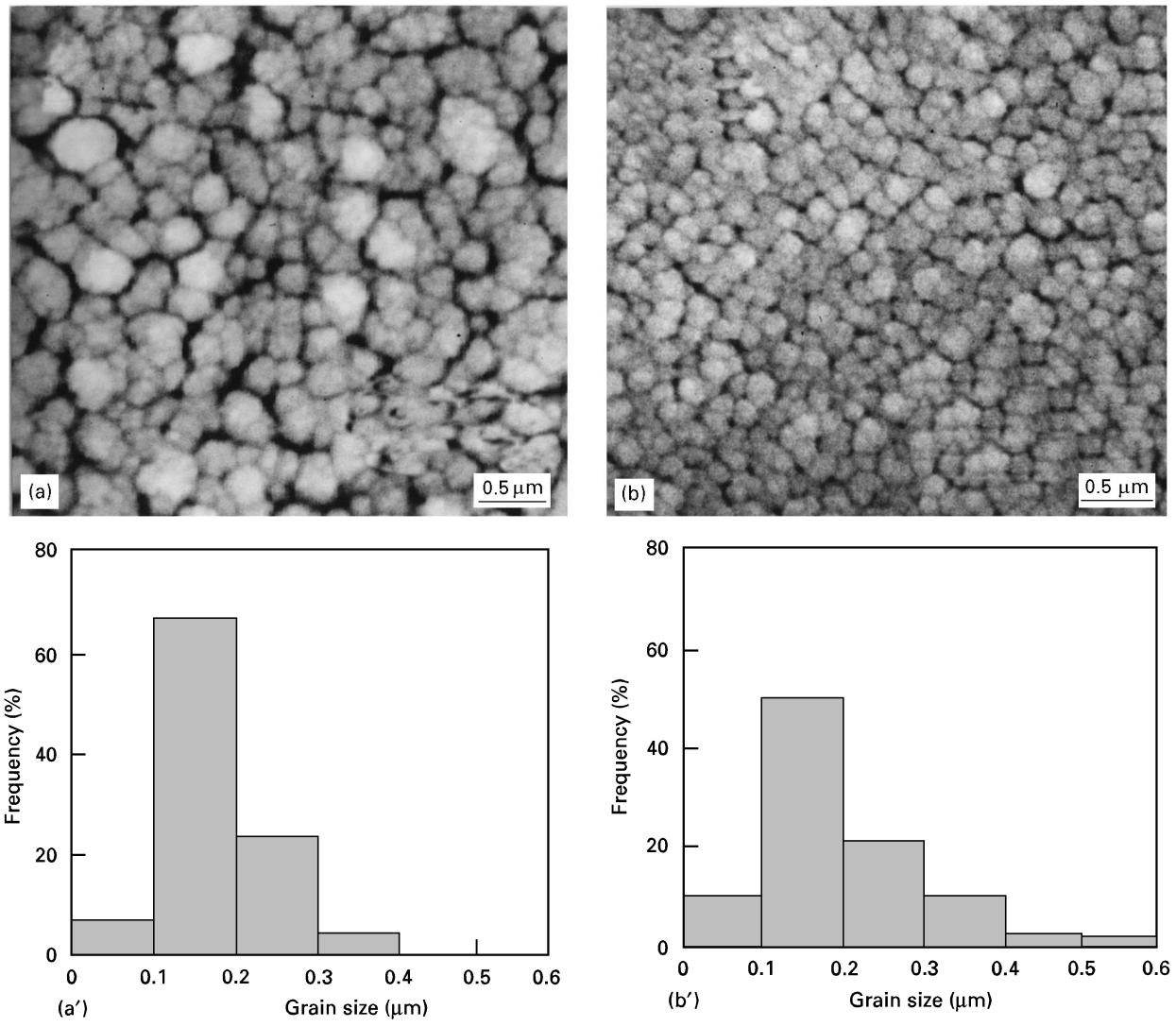

Figure 7 Typical SEM micrographs (above) and grain-size distributions (below) of Compact D(44) hot-pressed at 900 °C for (a) 1 h and (b) 3 h.

data at 1300 °C fell on another straight line. The data at 900 and 1100 °C are fitted to the following equation

$$dp^{0.28} = 0.51 \quad (5)$$

On the other hand, the data at 1100 °C are fitted to the following equation

$$dp^{0.10} = 23.1 \quad (6)$$

Thus the grain growth behaviours at 900 and 1100 °C may be different from the behaviour at 1300 °C. As described before, the sintering of primary particles at 900 °C occurs within secondary particles, following the rearrangement of secondary particles/grains. The sintering of grains at 1100 °C proceeds with eliminating the pores on the grain boundaries from the system. The grain growth at 900 and 1100 °C may thus be controlled by the pore migration on grain boundaries. On the other hand, the sintering of grains at 1300 °C proceeds along with the appreciable grain growth, due to the active mass transfer at this temperature.

4. Conclusion

The effect of starting particle size on hot-pressing of magnesium oxide (MgO) powder was examined using seven kinds of MgO powders prepared by a vapour phase oxidation process; the mean primary particle sizes of these powders were 11, 25, 32, 44, 57, 107 and 261 nm. These compressed powders (compacts) were hot-pressed at each temperature of 900 °C for 3 h, 1100 °C for 1 h and 1300 °C for 1 h. The results obtained can be summarized as follows:

1. The densifications of the compacts during the hot-pressing at 900 °C proceeded via the sintering of primary particles within secondary particles and the rearrangement of secondary particles/grains. Although gradual grain growth occurred at 900 and 1100 °C, rapid grain growth occurred at 1300 °C. The grain sizes of MgO compacts hot-pressed at and below 1100 °C were < 1 μm, while those at 1300 °C attained 20 $\sim$ 30 μm.
2. When the compact with the average primary particle size of 44 nm was hot-pressed at a temperature as low as 1100 °C, the translucent compact with the relative density of 99.7 % could be obtained.

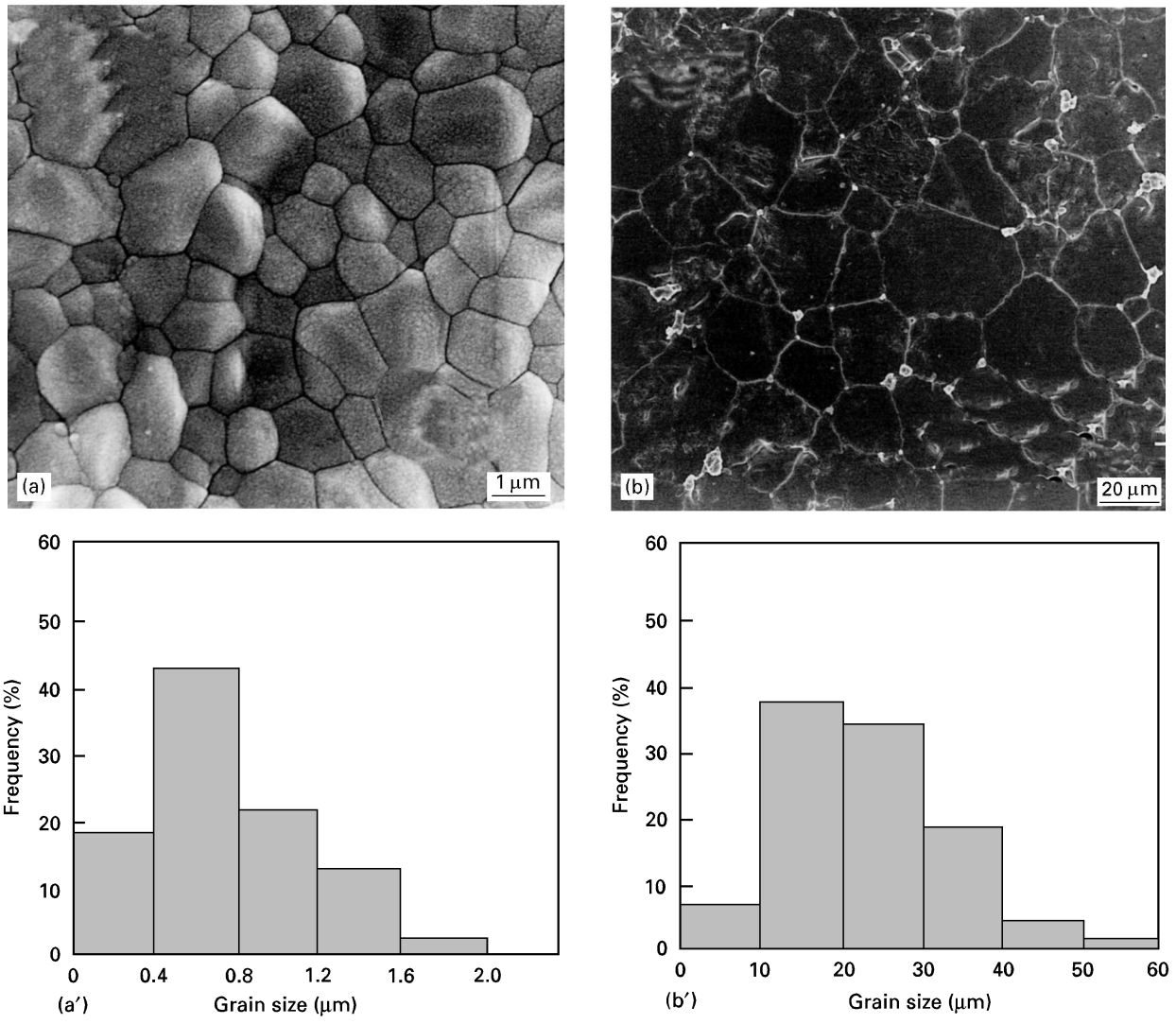

Figure 8 Typical SEM micrographs (above) and grain-size distributions (below) of Compact D(44) hot-pressed at (a) 1100 °C for 1 h and (b) 1300 °C for 1 h.

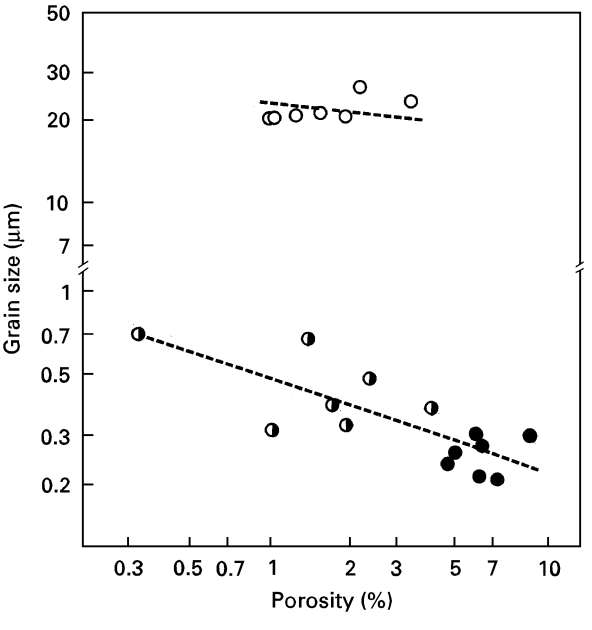

Figure 9 Relationship between grain size and porosity of the hot-pressed compact. (●) 900 °C, 3 h; (◑) 1100 °C, 1 h; (○) 1300 °C, 1 h.

Acknowledgements

The authors wish to express their thanks to Ube Industries Ltd. for providing the sample powders and to Mr. T. Murata of Nikon Corp. for measuring the agglomerate size distribution.

References

1. K. ITATANI, A. KISHIOKA and M. KINOSHITA, *Gypsum & Lime* **244** (1993) 4.
2. K. ITATANI, M. NOMURA, A. KISHIOKA and M. KINOSHITA, *J. Mater. Sci.* **21** (1986) 1429.
3. K. ITATANI, A. ITOH, F. S. HOWELL, A. KISHIOKA and M. KINOSHITA, *ibid.* **28** (1993) 719.
4. A. ITOH, K. ITATANI, A. KISHIOKA and M. KINOSHITA, *ibid.* **31** (1996) 2757.
5. K. YASUDA, S. KIM, Y. KANEMICHI, Y. MATSUO and S. KIMURA, *J. Ceram. Soc. Jpn* **90** (1990) 1103.
6. R. L. FULLMAN, *Trans. AIME* **197** (1953) 447.
7. T. YAMAGUCHI, *Bull. Ceram. Soc. Jpn* **17** (1982) 1074.
8. A. NISHIDA, A. UEKI, K. YOSHIDA, in "Advances in ceramics Vol. 21: Ceramic powder science", edited by G. L. Messing, K. S. Madzdiyasni, J. W. McCauley and R. A. Haber (The American Ceramic Society, Westerville OH, 1987) p. 271.
9. D. L. JOHNSON and I. B. CUTLER, *J. Amer. Ceram. Soc.* **46** (1963) 541.

10. F. R. WERMUTH and W. J. KNAPP, *ibid.* **56** (1973) 401.
11. K. HAMANO, K. YOSHINO and H. TOGANO, *Yogyo-Kyokai-Shi* **74** (1966) 312.
12. O. YAMAGUCHI, H. TONAMI, T. HAYASHI and K. SHIMIZU, *J. Jpn. Soc. Metals and Metall.* **24** (1977) 157.
13. W. D. KINGERY and M. BERG, *J. Appl. Phys.* **26** (1955) 1205.
14. W. H. RHODES, *J. Amer. Ceram. Soc.* **64** (1981) 19.
15. R. M. SPRIGGS and T. VASILOS, *J. Amer. Ceram. Soc.* **46** (1963) 224.
16. R. C. LOWRIE, JR. and I. B. CUTLER, in "Sintering and related phenomena", edited by G. C. Kuczynski, N. A. Hooton and C. F. Gibbon (Gordon and Breach, Science Publishers, New York, 1967) p. 527.
17. P. RAMAKRISHNAN, *Trans. Brit. Ceram. Soc.* **67** (1968) 135.
18. G. R. TERWILLIGER, H. K. BOWEN and R. S. GORDON, *J. Amer. Ceram. Soc.* **53** (1970) 241.
19. M. H. LEIPOLD and C. M. KAPADIA, *J. Amer. Ceram. Soc.* **56** (1973) 200.
20. W. BEERE, *J. Mater. Sci.* **10** (1975) 1434.
21. J. M. VIEIRA and R. J. BROOK, *J. Amer. Ceram. Soc.* **67** (1984) 450.
22. G. C. KUCZYNSKI, *Mater. Sci. Monogr.* **8** (1981) 44.

Received 27 February
and accepted 13 November 1996